Minerals Engineering 173 (2021) 107183

Contents lists available at ScienceDirect

Minerals Engineering

journal homepage: www.elsevier.com/locate/mineng

An investigation on hydrofluoric (HF) acid-free extraction for niobium oxide (Nb_2O_5) and tantalum oxide (Ta_2O_5) from columbite/tantalite concentrates using alkali reductive roasting

Steven Ghambi [a,d], Sergio Sanchez-Segado [b,d,*], Vitalis Chipakwe [c,d], Animesh Jha [d]

[a] University of Malawi-The Polytechnic, Department of Mining Engineering, P/Bag 303 Chichiri, Blantyre 3, Malawi
[b] Department of Chemical and Environmental Engineering, Technical University of Cartagena, Cartagena 30202, Spain
[c] Minerals and Metallurgical Engineering, Department of Civil, Environmental and Natural Resources Engineering, Luleå University of Technology, Luleå, Sweden
[d] School of Chemical and Process Engineering, University of Leeds, Leeds LS2 9JT, United Kingdom

ARTICLE INFO

Keywords:
Tantalum
Niobium
Carbothermic reduction
Roasting
Tantalite minerals

ABSTRACT

Tantalum, niobium, and their oxides are important precursor materials, essential for high-temperature alloys and electronic devices. The primary hydrometallurgical extraction technique to extract tantalum and niobium from minerals involves hydrofluoric acid (HF) digestion of the concentrates, followed by solvent extraction as an oxide separation and purification step. Solvent extraction, on the other hand, releases organic solvents which are lost irreversibly via natural evaporation during the process. This research demonstrates a novel chemical process for the extraction and refining of columbite and tantalite concentrates (29% Ta_2O_5 and 16% Nb_2O_5). In this process, the concentrates are reduced using carbon and alkali in the temperature range of 800–950 °C, which helps in reducing and magnetically separating the iron oxides present in the concentrates as metallic iron. The remaining residue is rich in alkali complex (e.g., sodium tantalates and niobates) formed during the roasting process which was reclaimed as a purified mixture of oxides of Nb_2O_5 and Ta_2O_5, by using oxalic acid leaching, followed by sodium bisulphate roasting.

1. Introduction

Niobium, tantalum, and their oxides are considered strategic materials due to being key components in the manufacturing of energy devices and systems. Consequently, these two metals remain in large demand for developing advanced structural steels (Moreno, 2011), nuclear (El-Genk and Tournier, 2005) and aerospace alloys (Upadhya et al., 1997). Their oxides are also widely used in the manufacturing of capacitors. The largest end-use market for niobium is in HSLA (high strength, low alloy) steel, for which the demand is expected to grow at 5–7% per year in the building and construction sector (Moreno, 2011). By comparison, niobium and tantalum are essential alloying elements in aerospace alloys for enhancing high-temperature performance for reducing greenhouse gas (GHG) emissions by decreasing the fuel consumption (Maki et al., 1992; Upadhya et al., 1997). In nuclear reactors, niobium is particularly important because of its small capture cross-section for thermal neutrons. The presence of niobium helps in improving reactor life and enhances hydrogen transport which reduces the risk of structural failure due to the occlusion of gas in the alloy lattice. Another application of niobium and tantalum is in mobile and handheld communication devices. In addition, both of these metals are also physiologically innocuous, which enables them to be used in implants and prostheses (Ryan et al., 2006).

The columbite group minerals (CGM) are the main natural source to produce metallic Nb and Ta. CGM are a family of complex solid solutions with the general formula $A^{2+}B_2^{5+}O_6$, where A sites are mainly occupied by Fe^{2+} and/or Mn^{2+} and B sites by Nb^{5+} and/or Ta^{5+}. The chemical composition of the CGM can be represented using the quadrilateral diagram shown in Fig. 1 (Ercit et al., 1995; Santos et al., 2001).

The areas (1) and (2) correspond to phases with a triple stored α-PbO_2 structure (orthorhombic), which form a continuous series of solid solutions between columbite and tantalite, being rich in Nb and Ta elements, respectively. The $FeTa_2O_6$ corner represents the mineral tapiolite (area 3) with a tri-rutile crystal structure (tetragonal). The shaded area defines the compositional field in which both structures coexist as independent solid phases. The shape, extent, and location of

* Corresponding author at: Department of Chemical and Environmental Engineering, Technical University of Cartagena, Cartagena 30202, Spain.
E-mail addresses: sergio.segado@upct.es, s.sanchezsegado@leeds.ac.uk (S. Sanchez-Segado).

https://doi.org/10.1016/j.mineng.2021.107183
Received 29 March 2021; Received in revised form 28 July 2021; Accepted 1 September 2021
Available online 13 September 2021

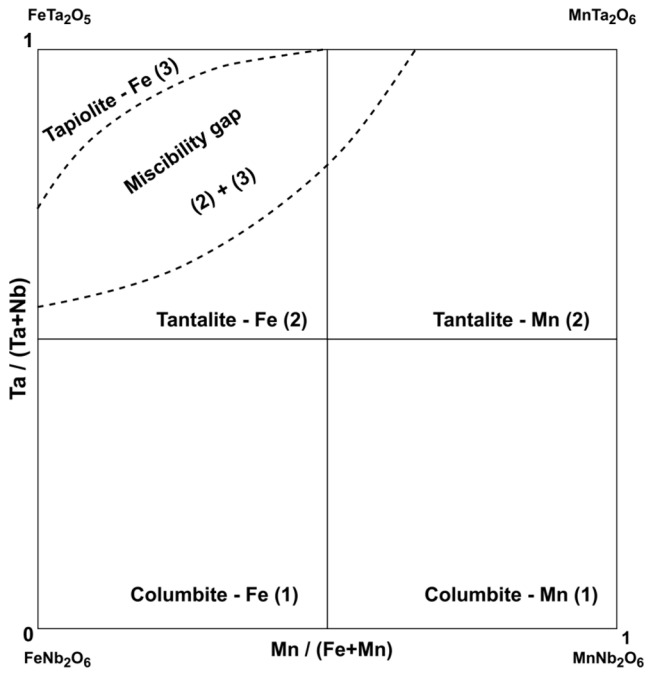

Fig. 1. Columbite group minerals quadrilateral diagram modified after (Ercit et al., 1995; Santos et al., 2001).

the two-phase region are controlled by temperature, pressure, the structural state of the co-existing phases and the presence of impurities (Wise, 1996; Mirão and Figueiredo, 2006). Tanaka et al. (Tanaka et al., 1988) investigated the system $FeTa_2O_6$-$MnTa_2O_6$ and found that Fe^{2+} can be replaced by Mn^{+2} up to 20 % mol and Nb^{5+} can also substitute Ta^{+5} with a solubility limit of 45 % mol in tapiolite.

The industrial treatment of CGM concentrates consists of the digestion of the concentrate using a mixture of sulphuric and hydrofluoric acid at temperatures between 250 and 300 °C to form niobium and tantalum fluorides, which are selectively separated by solvent extraction using organic solvents like ketones, large chain alcohols, cyclic hydrocarbons, amines, and phosphine compounds as shown in Fig. 2. The main drawbacks of the current technology are (Polyakov and Polyakova, 2003; Rodriguez et al., 2015; Zhu and Cheng, 2011):

1. Permanent loss of reagents during process operation
2. Generation of a huge amount of solid wastes. The production of 1 ton of oxides of niobium and tantalum generates 14 tons of solid wastes.
3. The recycling of HF involves serious environmental pollution and increases operating and energy costs.

To remove or minimize the use of HF in the process, chlorination, and carbo-chlorination with gaseous mixtures of N_2-Cl_2 and N_2-Cl_2-CO, the use of sodium salts as complexing agents in mixtures such as NaF-HF and $Na_2C_2O_4$-HF and digestion of the concentrates with NH_4NF_2 have been investigated (Brocchi and Moura, 2008; Gonzalez et al., 1998; Kabangu and Crouse, 2012; Mudzanapabwe et al., 2004; Rodriguez et al., 2016). These improvements have been focused on decreasing the amount of HF employed or its replacement for chlorine gas which still do not meet the sustainability criteria required in modern societies due to the toxic nature of chlorine gas and fluoride salts (Deblonde et al., 2019).

In recent investigations, oxidative roasting and high-temperature leaching with sodium and potassium-based alkali were adopted for demonstrating the reclamation of alumina, chromium, titanium, tantalum, niobium and rare-earth oxides (Deblonde et al., 2016; Escudero-Castejón et al., 2021; Sanchez-Segado et al., 2017, 2015, 2014; Wang et al., 2009; Zhou et al., 2005). As the global energy demand increases, more of such demands need to be met by developing efficient

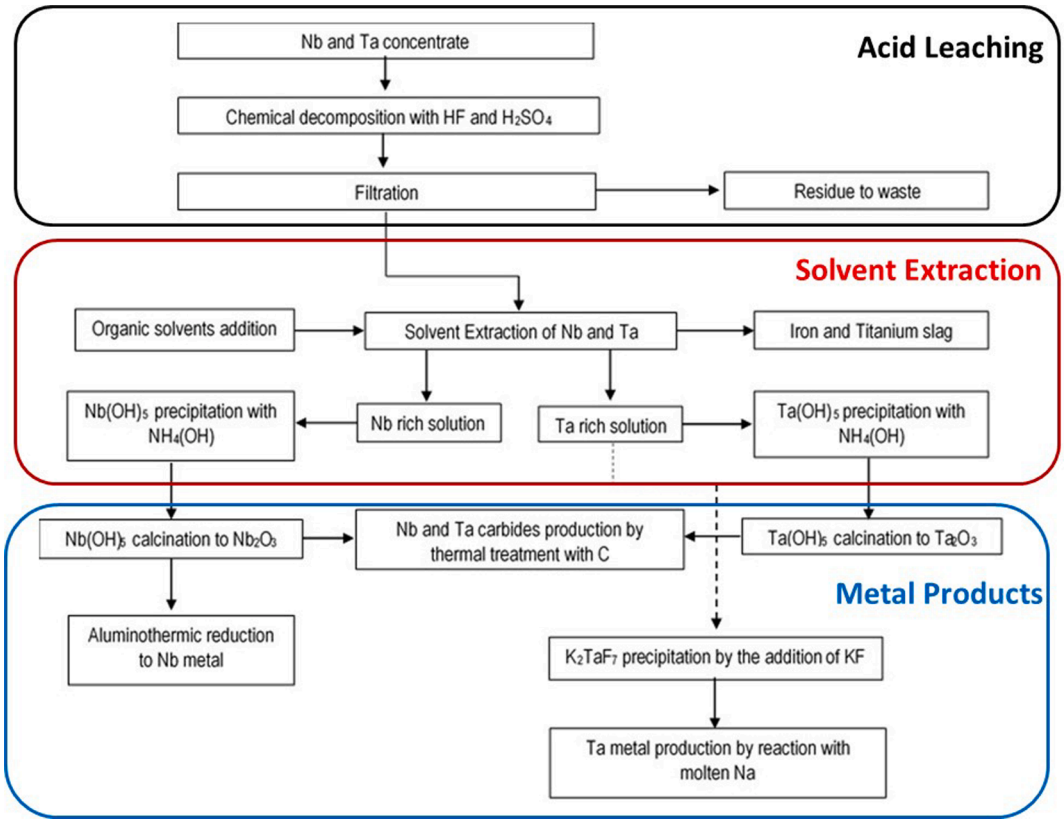

Fig. 2. Industrial processing of columbite concentrates flow chart.

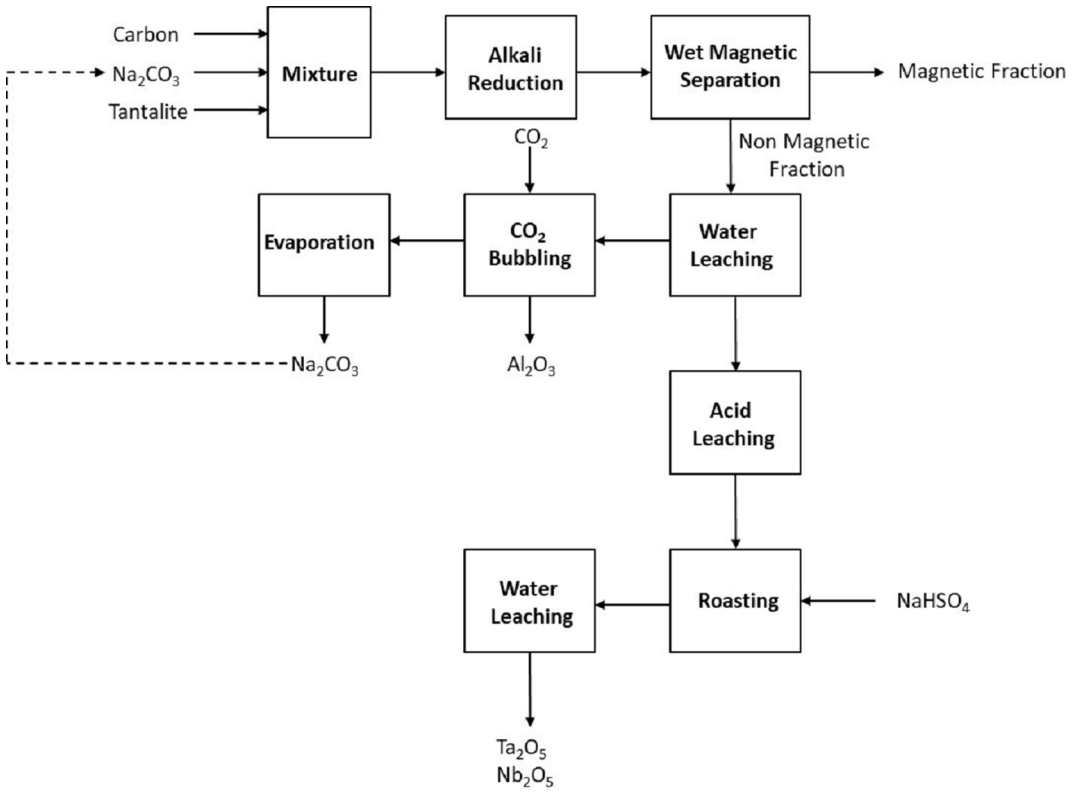

Fig. 3. Flow chart for the reductive alkali roasting treatment tantalite concentrates.

Table 1
Chemical composition of the as-received DRC tantalite concentrate.

	Weight percentage (%w/w)									
Oxide	Ta_2O_5	Fe_2O_3	Nb_2O_5	SiO_2	Al_2O_3	MnO	K_2O	SnO_2	TiO_2	Others*
	28.9	18.1	15.7	11.4	6.9	5.6	2.6	2.3	2.2	6.3

*oxides of Na, W, P, Pb, Zr, Sr, U, Cu, Zn, Sc, and V; each in minute concentrations.

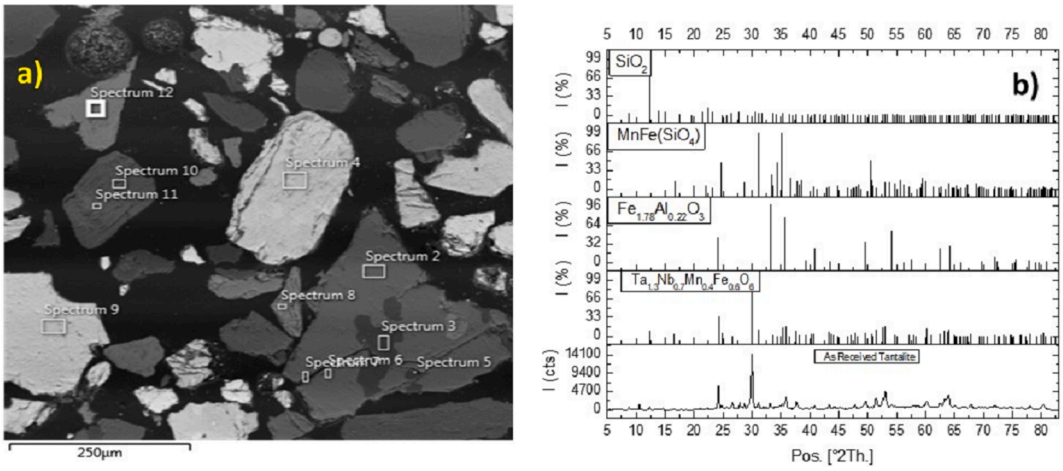

Fig. 4. Characterization of the as received tantalite mineral using (a) SEM (BSE) image and (b) XRPD pattern.

processing methods that generate less process effluents. For this reason, it is essential that the materials used for energy generation, like Ta and Nb, are also processed with a methodological approach, that is less energy taxing and environmentally damaging. Therefore, the development of efficient processes for metal extraction is of crucial importance for the protection of the environment.

In this article, a novel processing route for the treatment of CGM based on alkali roasting in reducing conditions is demonstrated to offer a potential alternative to the conventional process where HF is used. Specifically, we have demonstrated the feasibility of producing a

Table 2
EDX analysis of Fig. 4(a).

Element	Spectrum 2 (Wt.%)	Spectrum 3 (Wt.%)	Spectrum 4 (Wt.%)
O	33.2	46.9	17.7
Ta	–	–	43.3
Nb	–	–	20.8
Si	18.6	52.6	1.6
Fe	24.1	0.5	8.4
Al	11.8	–	–
Mn	7.3	–	5.8
Ca	3.8	–	–
Mg	1.3	–	–
W	–	–	1.4
Ti	–	–	0.9

mixture of purified Ta and Nb oxides by removing the impurities associated with CGM minerals such as manganese, aluminium, and silica to reduce downstream waste and to convert iron impurities into potentially saleable products. The Ta and Nb oxides obtained can then be used as feed for their respective metal/alloy production.

2. Experimental

2.1. Raw materials

The samples used in this study were supplied by the Tantalum-Niobium International Study Centre from the Democratic Republic of Congo (DRC). The as-received material was grounded using a FRITSCH Mortar Grinder PULVERISETTE 2 to achieve a finer homogenous feed with a particle size below 75 μm. All reagents used were of analytical grade and deionised water was used throughout.

2.2. Roasting and leaching tests

The ground sample was thoroughly mixed with alkali (Na_2CO_3) and carbon (activated charcoal) using variable concentrate: alkali: carbon weight ratios according to the stoichiometries based on reactions (1) to (5). The calculated stoichiometric concentrate: alkali: carbon weight ratio was 1:0.44:0.08. Mixtures were heated in a tube furnace under isothermal reducing conditions for 2.5 h, in argon atmosphere at 900 °C and 950 °C. Reduced samples were grounded below 75 μm and magnetically separated in a two-stage wet magnetic separation (WLIMS) process (Wet Test Chute from Master Magnets Ltd). The non-magnetic fraction formed was water leached at 60 °C for 1 h and subsequently leached in oxalic acid (0.5 M) at 60 °C for 2 h. After water leaching, the alkaline solution was bubbled with carbon dioxide to precipitate and recycle sodium carbonate. The acid leaching residue was dried and roasted with sodium bisulphate (1:1 mass ratio) at 650 °C for 1.5 h to produce enriched Ta_2O_5 and Nb_2O_5 and remove other metallic impurities. The flow chart of Fig. 3 summarises the procedure and steps described in this section.

2.3. Material characterization.

Solid samples were characterized using a Philips X'Pert X-ray diffractometer over a 2θ angle ranging from 5 to 85°, using Cu-Kα radiation for phase compositions. X'Pert HighScore Plus database software was used for phase identification of the X-ray Powder Diffractometry (XRPD) patterns. Scanning electron microscopy (SEM) including the use of energy-dispersive X-ray spectrometry (EDX) was used to study the microstructure using a Carl Zeiss Evo MA 15 scanning microscope at 20 kV.

2.4. Thermodynamic analysis of the reducing alkali roasting process.

The thermodynamic analysis of the roasting process in reducing conditions has been carried out using the commercial software HSC Chemistry 5.1 and Fact-Sage 7.1.

3. Results and discussion

3.1. Characterization of the as-received tantalite ore.

The chemical composition of the as-received tantalite concentrate is shown in Table 1. As it can be observed, the major components were Ta_2O_5, Fe_2O_3, Nb_2O_5, and SiO_2.

The X-ray Powder Diffraction (XRPD) pattern of the ore in Fig. 4 (b)

Table 3
Products of different stoichiometry for different reduction temperature.

T (°C)	*Ta:Na:C ratio	Mixture (g)	Roasted Mass (g)	*W-L (%)	*N-M (g)	*M−F (g)	N-M yield (%)	N-M Acid leached residue (g)
900 °C	1:0.44:0.08	46.6	33.9	27.1	17.3	10.8	57.7	6.9
	1:0.66:0.08	53.7	41.8	22.1	19.6	4.7	51.9	5.3
950 °C	1:0.44:0.08	46.6	36.8	21.0	19.3	10.4	59.0	8.1
	1:0.66:0.08	53.7	41.1	23.4	16.8	6.1	45.2	4.2

*Ta: Na:C = tantalite: sodium carbonate: carbon, W-L = weight loss, N-M: Non-Magnetic fraction, M−F = Magnetic fraction.

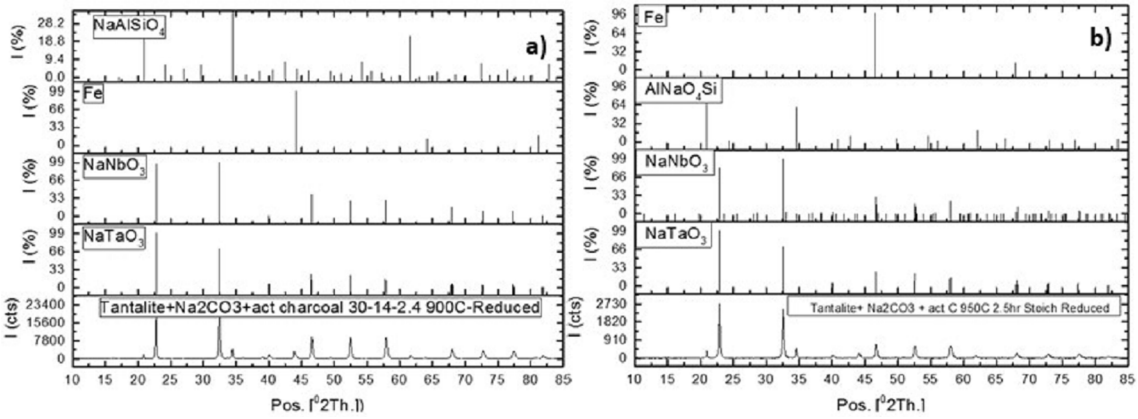

Fig. 5. XRPD pattern for stoichiometric reduced samples. (a) reduction at 900 °C (b) reduction at 950 °C.

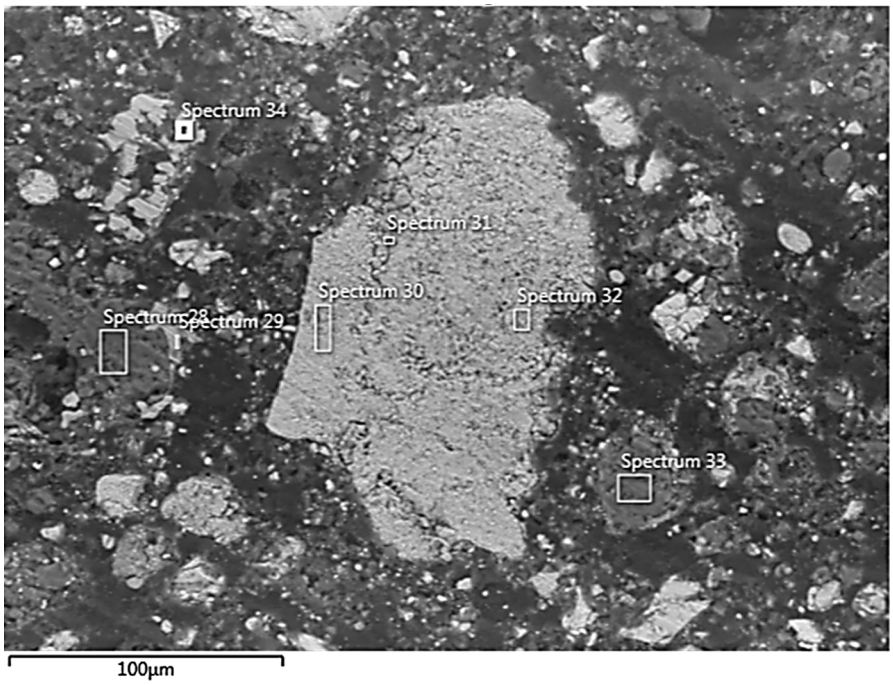

Fig. 6. SEM image (BSE) and EDX spectrums for reduced sample (reduced at 900 °C). Similar spectrums were observed for samples reduced at 950 °C.

Table 4
EDX analysis of the areas identified in Fig. 6.

Element	Spectrum 28 (Wt%)	Spectrum 30 (Wt%)	Spectrum 34 (Wt%)
O	35.3	23.2	3.0
Ta	–	37.3	1.7
Nb	–	15.2	–
Na	25.4	11.2	2.5
Si	14.4	3.7	–
Fe	0.9	3.2	87.9
Al	7.8	–	–
Mn	13.5	2.4	–
Ca	0.7	1.3	–
Mg	0.7	–	–
W	–	–	–
Ti	0.9	2.1	–
Sn	–	–	4.9

showed a close match with orthorhombic tantalite (ICDD reference code: 04–018-7027), silicon dioxide (ICDD reference code: 00–033-0659) and an orthorhombic silicate phase of manganese and iron (ICDD reference code: 04–013-6070). The SEM image in Fig. 4 (a) confirmed the existence of the observed orthorhombic tantalite phase, appearing as Ta, Nb, Fe and Mn existing in association in form of light grey phase as shown in EDX spectrum 4 of Table 2. The EDX analysis also showed that minor amounts of Si, W and Ti are invariably associated with the tantalite mineral phase. These observations are consistent with the work carried out by Santos et al. (2001). These minor substitutions could not be detected in the XRPD analysis of Fig. 4 (b) due to the XRPD technique is ineffective at detecting phases at concentrations of less than 5 wt% (Vyverberg et al., 2018). It is also observable that a dark grey phase (EDX, Spectrum 3) exists in the sample which has been identified as SiO_2 by XRPD.

3.2. Reductive alkali roasting of the tantalite concentrate

In this study, stoichiometric and non-stoichiometric amounts of alkali were separately studied at the reduction temperatures of 900 °C and 950 °C. Reduction results are tabulated in Table 3.

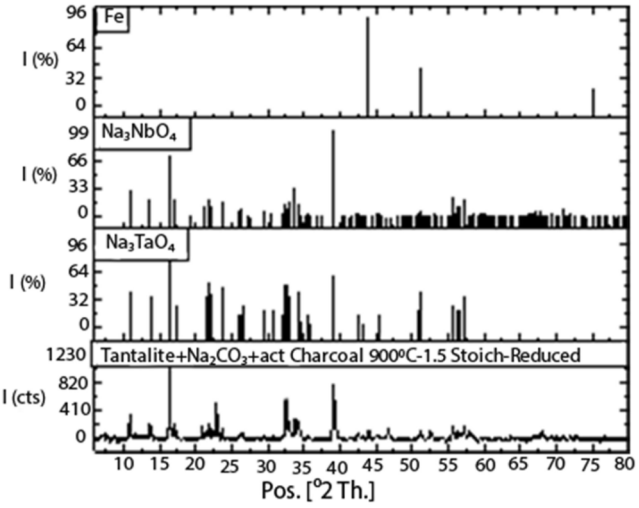

Fig. 7. XRPD pattern for tantalite sample reduced at 900 °C using 1.5 stoichiometric amounts of Na_2CO_3. (Notice how the phases are different from the stoichiometric sample).

3.2.1. Influence of the roasting temperature

In the present study, the roasting temperature was varied to investigate its influence on the evolution of alkali salts of tantalum and niobium, and other constituents like aluminium, iron, and manganese. XRPD patterns for both roasting temperatures (900 °C and 950 °C) for a stoichiometric sample are shown in Fig. 5. Similar results were obtained for the roasting using 1.5 times the stoichiometric amount of sodium carbonate.

It is clear from Fig. 5 that there is no added advantage in terms of the type of species that evolve, by conducting the reductive roasting at temperatures higher than 900 °C. In addition, Table 3 suggests that higher roasting temperatures do not produce an appreciably different mass yield of the non-magnetic portion containing the valuable tantalum and niobium alkali salts. In fact, the percentage yield was observed to be lower at a higher roasting temperature than at the lower

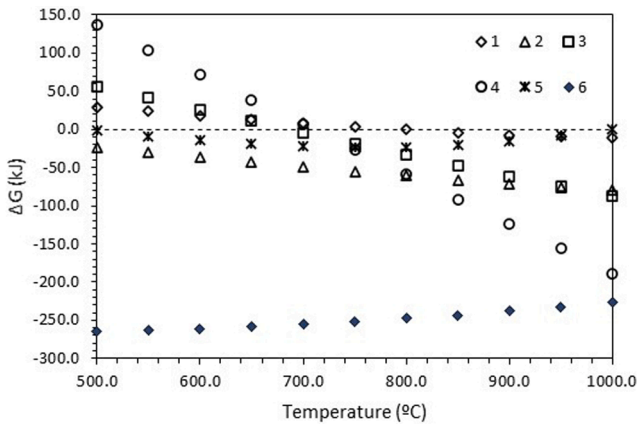

Fig. 8. Evolution of ΔG with temperature for reactions (1) to (6). The dashed line represents ΔG = 0.

one. SEM images and EDX spectrums shown in Fig. 6 corroborate the existence of the phases shown in Fig. 5. In Table 4, which captures the EDX spectrum of Fig. 6, the elemental content values are quoted in weight percent (wt.%). A valuable observation from Fig. 6 is that the Iron (Fe) phase (spectrum 34) is physically separate from the alkali salts of interest, $NaTaO_3$ and $NaNbO_3$ (spectrum 30). This means that with appropriate size reduction through grinding, Fe can theoretically be separated from the alkali salts by a magnetic separation technique.

3.2.2. *Influence of the alkali concentration*

The influence of the alkali content was also investigated to assess the chemical and physical changes occurring during the alkali reduction of tantalite. Stoichiometric and 1.5 times stoichiometric amounts of alkali were investigated for reduction at 900 °C. Results shown in Fig. 7 indicated that alkali salt matched closely with monoclinic Na_3TaO_4 (ICDD reference code: 00–027-1421) and monoclinic Na_3NbO_4 (ICDD reference code: 04–013-3712). These phases have also been reported by Sanchez-Segado et al. (2015) during the oxidative roasting of pure Ta_2O_5 and Nb_2O_5 using two times the stoichiometric amount of NaOH. These results indicate that a crystallographic change can be triggered in the products even when relatively low excess alkali is used. Moreover, in reference to Table 3, it is observed that using excess alkali amount during reduction lowered the mass yield of the magnetic fraction. This could be a result of low silicate amounts in the sample, thereby encouraging retention of Ta and Nb alkali salts in the magnetic fraction.

3.2.3. *Thermodynamics of the reductive roasting process*

According to the experimental roasting results for the stoichiometric amount of Na_2CO_3, reactions (1) to (6) have been identified to take place during the reduction process. The Gibbs free energy change (ΔG) of these reactions against temperature were computed using HSC 5.1

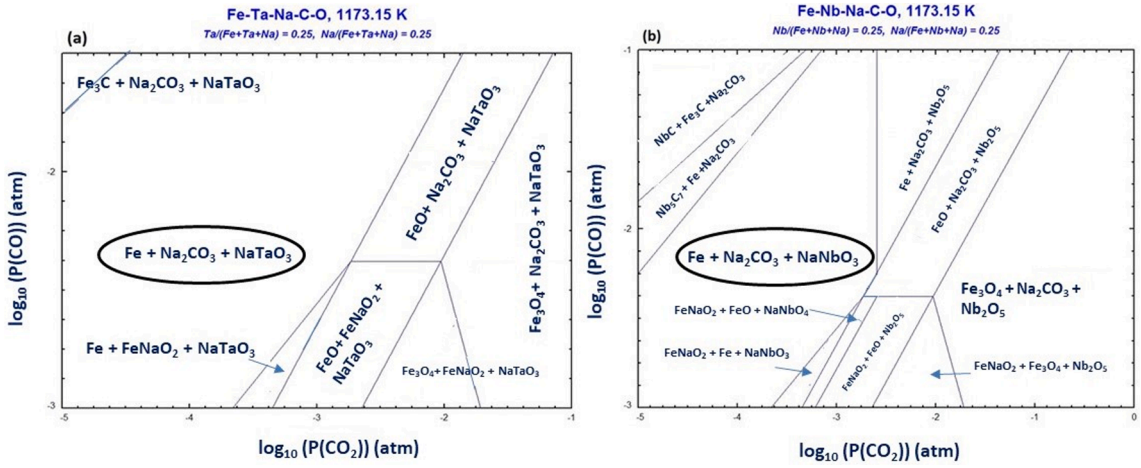

Fig. 9. a) Predominance area diagram for Fe-Ta-Na-C-O system at 1173.15 K (900 °C). b) Predominance area diagram for Fe-Nb-Na-C-O system at 1173.15 K (900 °C).

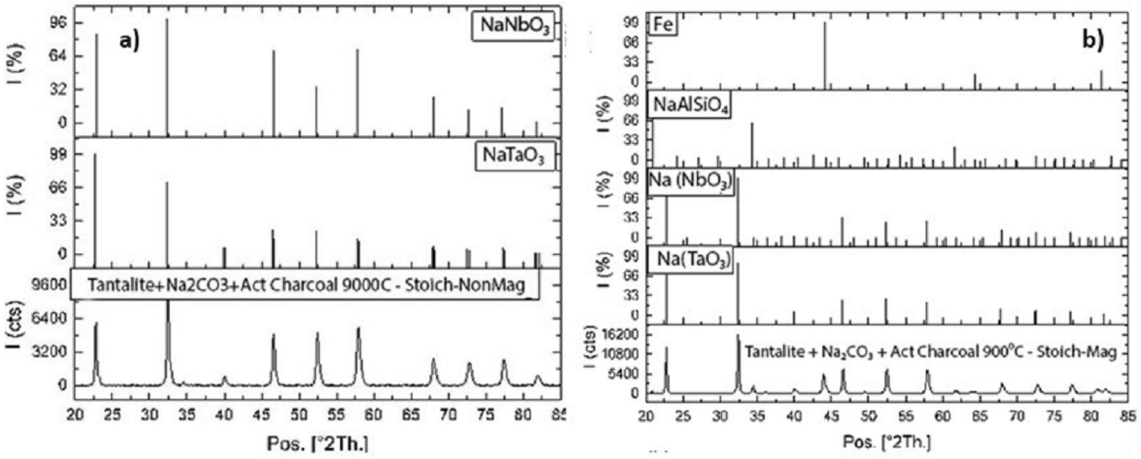

Fig. 10. XRPD patterns for (a) non-magnetic (b) magnetic fraction for stoichiometric sample reduced at 900 °C.

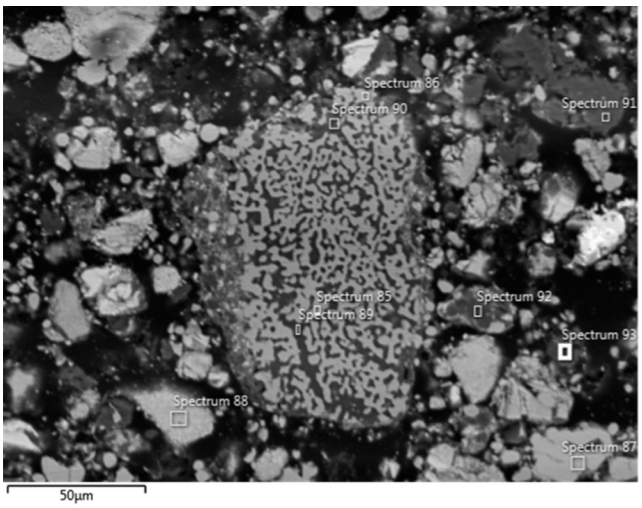

Fig. 11. SEM image (BSE) of magnetic fraction showing a spongy particle housing both magnetic and non-magnetic constituents.

Table 5
EDX analysis of Fig. 11.

Element	Spectrum 85 (Wt%)	Spectrum 88 (Wt%)	Spectrum 89 (Wt%)
O	1.8	20.3	32.6
Ta	–	38.4	–
Nb	–	18.2	–
Si	0.9	2.6	12.6
Fe	89.8	5.9	5.6
Al	0.4	0.3	9.6
Mn	1.1	2.0	9.5
Ca	–	0.6	0.3
Mg	–	–	0.7
W	–	0.6	–
Ti	–	0.5	0.1
Sn	4.8	1.8	0.6
Na	1.1	8.8	20.8
C	–	–	4.7
K	–	–	0.2

software and are plotted in Fig. 8.

$$Al_2O_3 + Na_2CO_3 \rightarrow 2NaAlO_2 + CO_{2(g)} \quad (1)$$

$$SiO_2 + Na_2CO_3 \rightarrow Na_2SiO_3 + CO_{2(g)} \quad (2)$$

$$TiO_2 + Na_2CO_3 + C \rightarrow Na_2O{*}TiO_2 + 2CO_{(g)} \quad (3)$$

$$Fe_3O_4 + 4C \rightarrow 3Fe + 4CO_{(g)} \quad (4)$$

$$Nb_2O_5 + Ta_2O_5 + 2Na_2CO_3 + 2C \rightarrow NaNbO_3 + NaTaO_3 + 4CO_{(g)} \quad (5)$$

$$MnO + 1/2Na_2CO_3 + 2CO_{2(g)} \rightarrow NaMnO_4 + 5/2CO_{(g)} \quad (6)$$

Fig. 8 was employed for predicting thermodynamically favourable reduction conditions and for the confirmation of the evolved phases. It is clear from the figure that the free energy values for reactions (1) to (6) are negative at temperatures above 850 °C approximately. The stability of the products formed after roasting in reducing conditions in the temperature range studied follows the sequence: $NaMnO_4$ > Fe > Na_2SiO_3 > $Na_2O{*}TiO_2$ > $NaNbO_3/NaTaO_3$ > $NaAlO_2$. The formation of $NaNbO_3$, $NaTaO_3$, $NaAlO_2$ and Na_2SiO_3 is desirable for the alkali reduction process, as $NaNbO_3$ and $NaTaO_3$ can be separated from metallic Fe by magnetic separation to subsequently extract $NaMnO_4$, $NaNbO_3$, $NaTaO_3$. $NaAlO_2$ and Na_2SiO_3 are solubilised during magnetic separation and water leaching yielding an alkaline solution that can be further treated with $CO_{2(g)}$ to recover Na_2CO_3, SiO_2 and Al_2O_3 (Escudero-Castejón et al., 2021; S. Sanchez-Segado et al., 2015).

Predominance area diagrams were also employed to predict favourable conditions for the reduction of Iron and the evolution of other species of interest. Fig. 9(a) and 9(b) demonstrate that at appropriate partial pressures of CO and CO_2 metallic iron (Fe) and sodium salts of Ta and Nb can co-exist. The areas of interest in both figures have been highlighted by encircling the thermodynamically stable constituents. Although not shown here, similar predominance area diagrams for both Ta and Nb are obtainable for the reduction at 950 °C.

XRPD and SEM data reveal that the products predicted from thermodynamics are present in the roasted samples. From XRPD data of Fig. 5, it is evident that alkali salts of Ta and Nb were obtained in both reduction environments, matching closely with monoclinic $NaTaO_3$ (ICDD reference code: 04–017-3868) and cubic $NaNbO_3$ (ICDD reference code: 04–002-0021). As predicted thermodynamically, elemental iron is also found, matching closely with ICDD's α-iron (reference code:

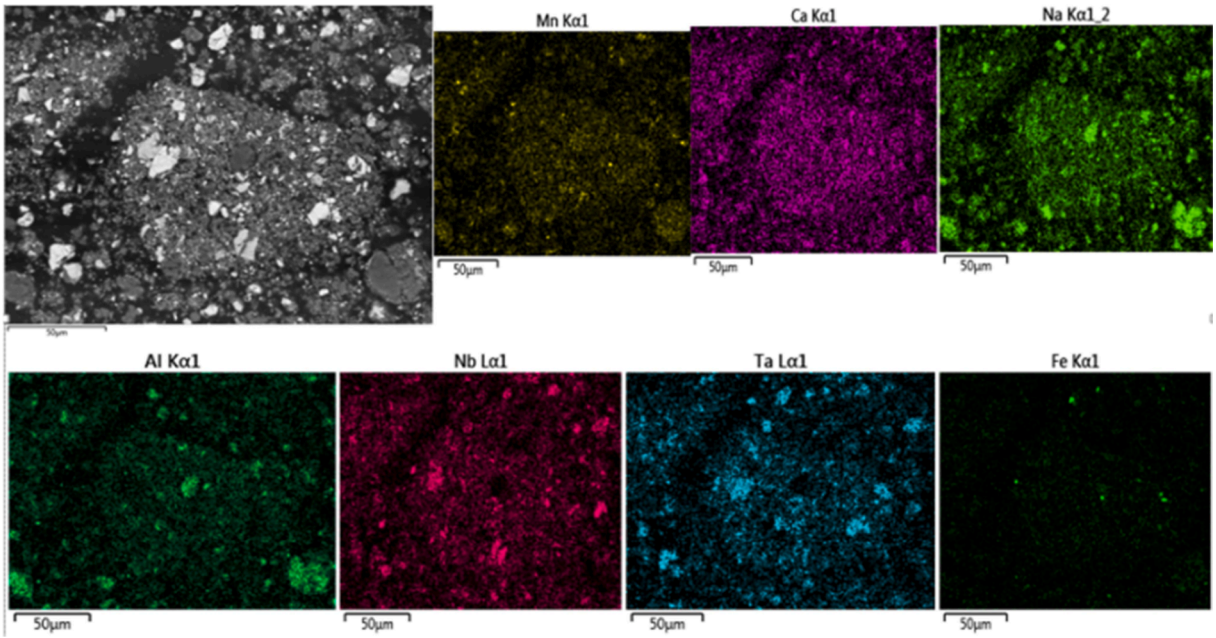

Fig. 12. Elemental map of the non-magnetic stream.

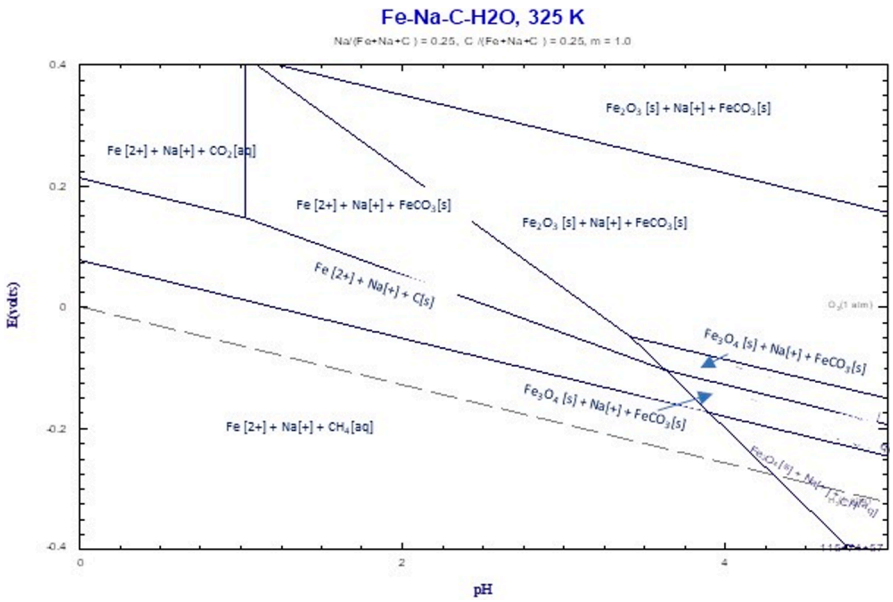

Fig. 13. Eh-Ph diagram for leaching iron from the non-magnetic fraction in tantalite processing.

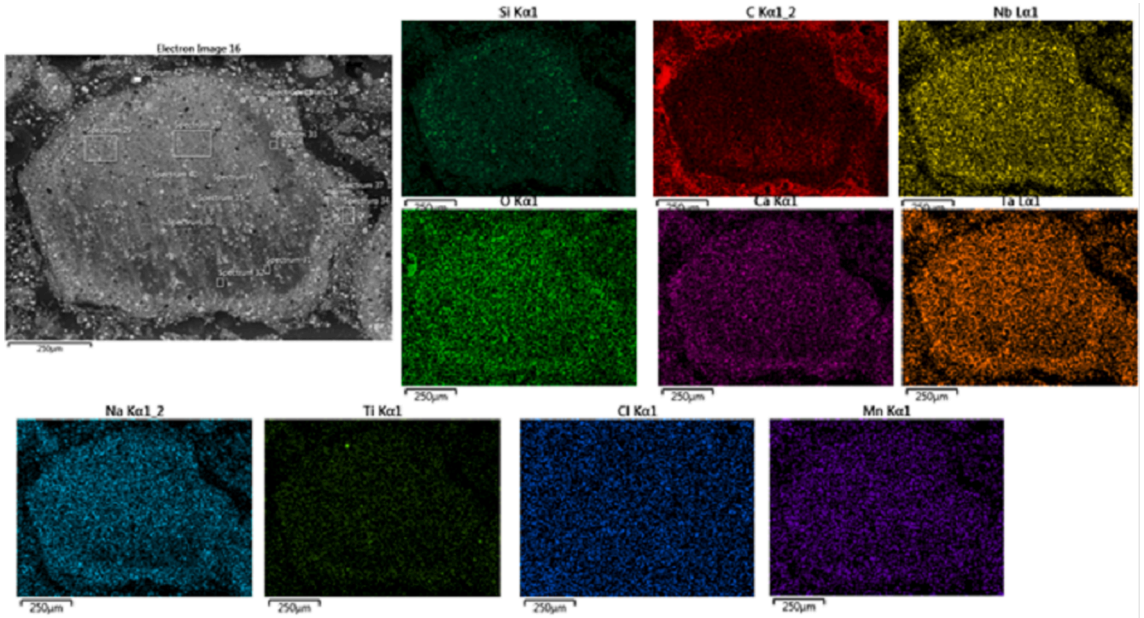

Fig. 14. Backscattered SEM image of the oxalic acid leaching residue.

01–080-3818). Although the match is close, there is a systematic phase shift, probably because of the incorporation of substitutional elements into the crystal structure of iron. This is visible in the EDX spectrum of Fig. 6 in which iron is associated with a small amount of tin. In other EDX spectrums, we observed that the reduced iron phase has a small inclusion of Mn and Ti. Finally, sodium aluminium silicate was also found to be a major phase existing in the reduced samples. Apart from confirming the existence of the aforementioned phases, the back-scattered SEM image and EDX spectrums of Fig. 6 indicate that the phases $NaNbO_3$ and $NaTaO_3$ occur as a solid solution.

3.2.4. *Wet magnetic separation*

The XRPD patterns for magnetic and non-magnetic fractions after separation are shown in Fig. 10. In Fig. 10a, it is observed that the magnetic fraction contains residual tantalum and niobium alkali salt phases. This also confirmed in the SEM image in Fig. 11 which reveals that some particles exhibit a sponge-like texture housing both alkali salts and metallic iron as corroborated by EDX data of Table 5. This suggests that they were not liberated fully, and further grinding was needed to physically liberate the alkali salts of tantalum and niobium from the iron particles. Theoretically, this can be solved by grinding the products of alkali reduction to very fine particles. Unfortunately, there is a practical limit to this in terms of fracture mechanics and energy consumption (Escudero-Castejon et al., 2017).

It was also observed that during wet magnetic separation, silicates of sodium and aluminium report mainly in the magnetic fraction as evident in the XRPD patterns of Fig. 10(a). It was also found, by SEM analysis, that small concentrations of silicates not identified in the XRPD patterns, for example, in Figs. 7 and 10a, were largely present in the non-magnetic fractions, as revealed in the EDX image in Fig. 11.

Since most of the iron had reduced to metallic form, no iron or manganese may likely be found with the silicate parts of the non-

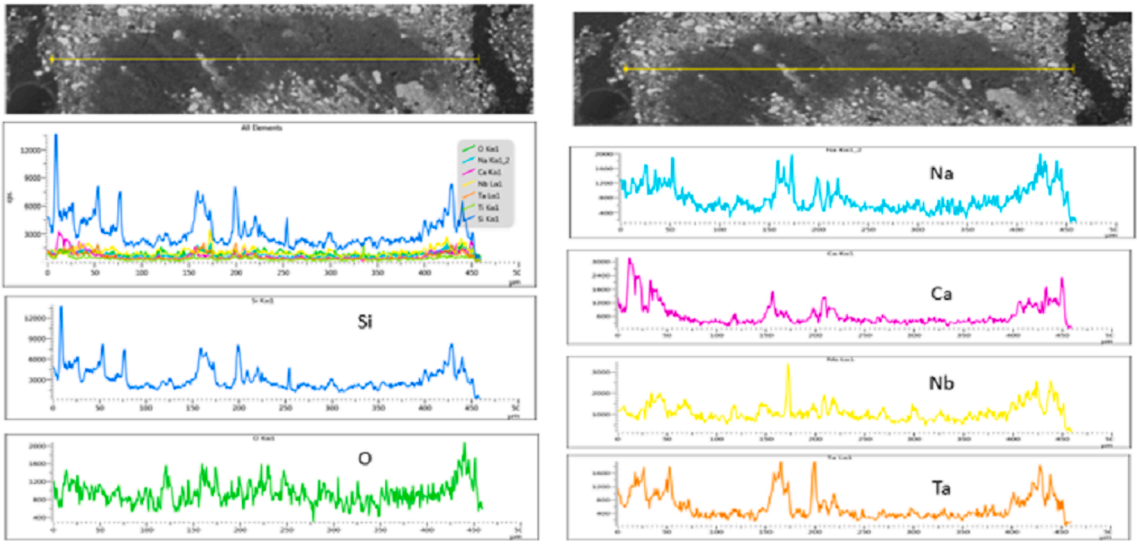

Fig. 15. Line scan of acid leach residue microstructure.

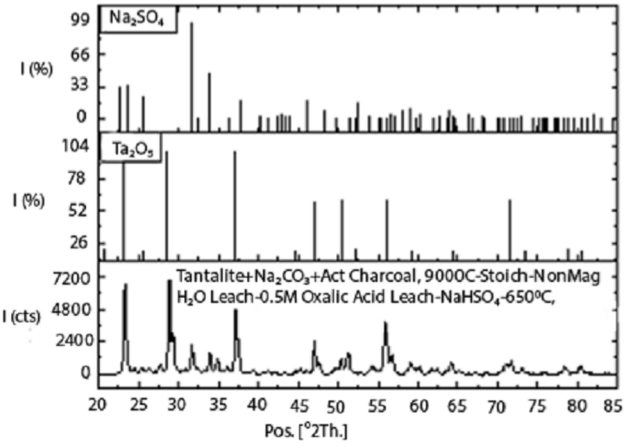

Fig. 16. XRPD showing phases of the product after reaction with sodium bisulphate.

magnetic fraction. Although SEM elemental maps of the same sample (Fig. 12) suggest that there are trace amounts of Fe reporting to the non-magnetic fraction, the inconspicuousness of the same in XRPD patterns indicates unsatisfactory field strength in the wet magnetic separation.

3.2.5. *Acid leach residue*

Oxalic acid leaching was carried out to remove iron impurities hosted in the non-magnetic fraction. For iron removal, the pH must be buffered below 4 to keep Fe^{2+} in solution as shown in the Eh-pH diagram in Fig. 13. Iron was removed from the sample through reaction (6) as

Table 6
EDX analysis of the areas identified in Fig. 16.

Element	Spectrum 16 (Wt%)	Spectrum 18 (Wt%)	Spectrum 21 (Wt%)
O	16.5	15.8	20.9
Ta	58.6	46.7	31.0
Nb	5.1	19.9	28.3
Si	3.4	2.4	2.7
Fe	–	1.2	–
Al	0.4	0.2	0.5
Mn	2.8	1.3	2.0
Ca	6.8	1.2	1.3
Mg	–	–	–
W	–	0.9	1.6
Ti	–	1.8	1.5
Sn	0.9	–	–
Na	5.4	8.7	10.2

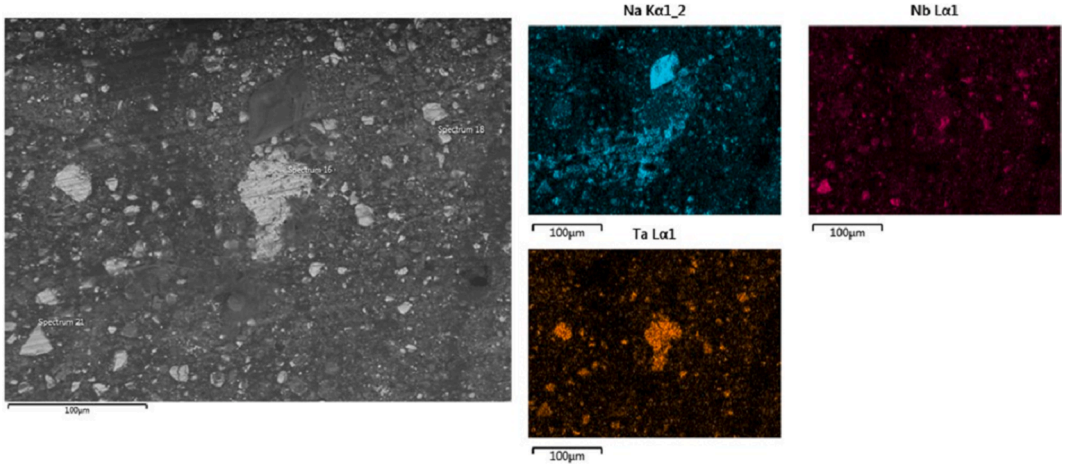

Fig. 17. SEM (BSE) and EDX spectrum confirming XRPD phases identified in products of reaction with sodium bisulphate.

Table 7
Energy analysis per tonne of concentrate.

Process Step	Energy Consumption (kWh/tn)
Reductive roasting	551.6
Magnetic Separation and water leaching	224.1
$CO_{2(g)}$ bubbling	219.0
Evaporation	138.9
Acid Leaching	128.9
Sodium bisulphate roasting	209.0

observed in the backscattered SEM image in Fig. 14.

$$Fe + H_2C_2O_4 \rightarrow FeC_2O_4 + H_{2(g)} \quad (6)$$

Additionally, the acid leaching steps provide more information on the spatial dissemination of elements in the microstructure. From the same Fig. 14, it is observed that silicon forms a "ring" around the core of the microstructure. It is also clear that in the bulk of the microstructure, the presence of carbon is limited, which suggests satisfactory reaction kinetics during the roast reaction time. The line scan provided in Fig. 15 further testifies the segregation of silicon to the peripheral of the microstructure as it recorded the highest cps values of the elements. It is also notable that there is more concentration of sodium niobate in the peripherals of the microstructure than sodium tantalite, despite the former being quantitatively less than the latter as reported in Table 5 above.

3.2.6. Production of Ta and Nb oxides

To transform the alkali salts of niobium and tantalum into their respective oxides, the acid leaching residue was roasted with sodium bisulphate according to equations (7) and (8).

$$NaHSO_4 + 2\ NaTaO_3 \rightarrow 2\ Na_2SO_4 + H_2O + Ta_2O_5 \quad (7)$$

$$2NaHSO_4 + 2NaNbO_3 \rightarrow 2\ Na_2SO_4 + H_2O + Nb_2O_5 \quad (8)$$

XRPD analysis of products from these reactions showed that indeed these products were obtained in the reaction. The major phases have been identified as Ta_2O_5 and Na_2SO_4 as shown in Fig. 16. The backscattered SEM image of Fig. 17 corroborates the existence of oxides of both Ta and Nb oxides as predicated by equations (7) and (8).

From the EDX analysis of Fig. 17 in Table 6, it can be depicted that niobium and tantalum oxides form a solid solution. The most stable form of Nb_2O_5 in the temperature range studied is the monoclinic α-Nb_2O_5 and for tantalum is the β-Ta_2O_5. The stable α-Nb_2O_5 is not isomorphic with the orthorhombic β-Ta_2O_5 which makes difficult the formation of mixed oxides despite the similarities of Nb^{5+} and Ta^{5+}. However, the metastable γ-Nb_2O_5 is isomorphic with β-Ta_2O_5 and exits at temperatures below 750–800 °C allowing the formation of a continuous series of solid solutions of both oxides (Zafrir et al., 1976). It is expected that during the slow air cooling of the samples these solid solutions formed in the roasted material.

3.2.7. Potential process benefits

The CGM process route reported in this article shows the following potential benefits:

1. The roasting of tantalite/columbite in reducing conditions, followed by oxalic acid leaching and further sodium bisulphate roasting helps in identifying a process for further refining to a concentration larger than 80% purity of Nb_2O_5-Ta_2O_5 mixture.
2. Current limitations of conventional HF leaching are due to acid loss (6–10 vol%) through volatilization (763 mm Hg pressure at 25 °C), generation of large amounts of acid wastewater containing fluoride salts. Such fluoride wastes contain reactive heavy metals which pose a major challenge in terms of safe disposal and management of the environment and personnel.
3. The reductive alkali roasting process presented in this work offers an alternative solution to the use of HF. The estimated energy consumption per ton of mineral of the process is presented in Table 7.

A total of 1471.5 kWh/tn are required in case that no energy recovery step is considered. However, the following energy recovery steps have been identified:

- The reductive alkali roasting offers the opportunity for utilizing CO and CO_2 off-gases by combustion of CO gas through the reaction $CO_{(g)} + 0.5O_{2(g)} \rightarrow CO_{(g)}$, the energy released from the complete combustion of CO gas is estimated to be 581.7 kWh/tn at 825 °C.
- Carbon dioxide is bubbled at 60 °C in the alkali recovery step. Thus, the off-gas cooling from 825 °C to 60 °C allows a maximum recovery of 256.5 kWh/tn.
- The solid product obtained after reductive roasting is cooled from 900 to 60 °C before going into the wet magnetic separation step allowing a maximum energy recovery of 351.2 kWh/tn. Considering these energy recovery steps, the theoretical energy consumption of the process is 282.1 kWh/tn.
- The estimated CO_2 emissions after combustion are 445.5 kg/tn. The CO_2 generated in the combustion can be bubbled to recover Na_2CO_3 and precipitate aluminium and silicon with a theoretical CO_2 consumption of 101.8 kg/tn

A comparison between the reductive alkali roasting and the conventional HF leaching process in terms of energy consumption and CO_2 emissions was difficult to undertake, as we have not found any representative data in the literature for the leaching process to properly address these questions.

4. Finally, the production of a magnetic fraction which mainly consists of metallic iron, can be sold to the steel industry, reducing waste generation, and increasing the process revenue.

4. Conclusions

The present work has demonstrated the possibility of processing tantalite minerals into tantalum and niobium oxides using a process based on the carbothermic reduction of tantalite ore with solid carbon (activated charcoal) in the presence of alkali in the temperature range of 800 °C to 950 °C without the use of hydrofluoric acid. The wet magnetic separation of reduced samples yields a nonmagnetic fraction residue which is the main source of sodium niobates and tantalates. Oxalic acid leaching of the niobates and tantalates was carried out to remove the remaining iron impurities. Further sodium bisulphate roasting of the acid leached residue yielded a mixture of Ta_2O_5-Nb_2O_5 solid solutions. Optimization of the different steps of the process is now required, with special emphasis on the separation of iron from sodium niobates and tantalates during wet magnetic separation and further purification of the mixed Ta_2O_5-Nb_2O_5 oxides.

CRediT authorship contribution statement

Steven Ghambi: Methodology, Investigation. **Sergio Sanchez-Segado:** Methodology, Investigation. **Vitalis Chipakwe:** Methodology, Investigation. **Animesh Jha:** Supervision.

Declaration of Competing Interest

The authors declare that they have no known competing financial interests or personal relationships that could have appeared to influence the work reported in this paper.

Acknowledgements

The authors acknowledge the support received from Stephen Parirenyatwa, Lidia Escudero Castejón, Ayoub Al-Selwi, Jennifer Forrester, and all members of Leeds Electron Microscopy and Spectroscopy Centre (LEMAS) for their help in the XRD and SEM analysis. The authors also wish to acknowledge the financial support received from the EPSRC standard grants (GR/T19889/01 and GR/L95977/01), the NERC SoS minerals grant (NE/M01147X/1), the NERC's Catalyst Grant reference NE/L002280/1, the European Union's Marie Curie Fellowship number 331385 granted to Dr Sanchez-Segado.

References

Brocchi, E.A., Moura, F.J., 2008. Chlorination methods applied to recover refractory metals from tin slags. Miner. Eng. 21 (2), 150–156. https://doi.org/10.1016/j.mineng.2007.08.011.

Deblonde, G.J.P., Bengio, D., Beltrami, D., Bélair, S., Cote, G., Chagnes, A., 2019. A fluoride-free liquid-liquid extraction process for the recovery and separation of niobium and tantalum from alkaline leach solutions. Sep. Purif. Technol. 215, 634–643. https://doi.org/10.1016/j.seppur.2019.01.052.

Deblonde, G.-J.-P., Weigel, V., Bellier, Q., Houdard, R., Delvallée, F., Bélair, S., Beltrami, D., 2016. Selective recovery of niobium and tantalum from low-grade concentrates using a simple and fluoride-free process. Sep. Purif. Technol. 162, 180–187. https://doi.org/10.1016/j.seppur.2016.02.025.

El-Genk, M.S., Tournier, J.-M., 2005. A review of refractory metal alloys and mechanically alloyed-oxide dispersion strengthened steels for space nuclear power systems. J. Nucl. Mater. 340, 93–112. https://doi.org/10.1016/j.jnucmat.2004.10.118.

Ercit, T., Wise, M., Černý, P., 1995. Compositional and structural systematics of the columbite group. Am. Mineral. 80, 613–619.

Escudero-Castejon, L., Sanchez-Segado, S., Parirenyatwa, S., Hara, Y., Jha, A., 2017. A cr6 +-free extraction of chromium oxide from chromite ores using carbothermic reduction in the presence of alkali. In: Applications of Process Engineering Principles in Materials Processing. Energy and Environmental Technologies, The Minerals, Metals & Materials Series, pp. 179–188.

Escudero-Castejón, L., Taylor, J., Sánchez-Segado, S., Jha, A., 2021. A novel reductive alkali roasting of chromite ores for carcinogen-free Cr6+-ion extraction of chromium oxide (Cr2O3) – A clean route to chromium product manufacturing! J. Hazard. Mater. 403, 123589 https://doi.org/10.1016/j.jhazmat.2020.123589.

Gonzalez, J., Gennari, F., Bohé, A., Ruiz, M. del C., Rivarola, J., Pasquevich, D., 1998. Chlorination of niobium and tantalum ore. Thermochim. Acta 311 (1–2), 61–69. https://doi.org/10.1016/S0040-6031(97)00376-6.

Kabangu, M.J., Crouse, P.L., 2012. Separation of niobium and tantalum from Mozambican tantalite by ammonium bifluoride digestion and octanol solvent extraction. Hydrometallurgy 129-130, 151–155. https://doi.org/10.1016/j.hydromet.2012.06.008.

Maki, K., Shioda, M., Sayashi, M., Shimizu, T., Isobe, S., 1992. Effect of silicon and niobium on oxidation resistance of TiAl intermetallics. Mater. Sci. Eng. A 153, 591–596. https://doi.org/10.1016/0921-5093(92)90256-Z.

Mirão, J.P., Figueiredo, M.O., 2006. Pattern of minor element enrichment in columbites: A synchrotron radiation X-ray fluorescence (SRXRF) study. Chem. Geol. 225, 402–410. https://doi.org/10.1016/j.chemgeo.2005.08.031.

Moreno, L., 2011. Tantalum and niobium primer-two critical materials.

Mudzanapabwe, N.T., Chinyamakobvu, O.S., Simbi, D.J., 2004. In situ carbothermic reduction of a ferro-columbite concentrate in the recovery of Nb and Ta as metal matrix composite from tin smelting slag waste dump. Mater. Des. 25 (4), 297–302. https://doi.org/10.1016/j.matdes.2003.10.015.

Polyakov, E.G., Polyakova, L.P., 2003. Current Trends in the Production of Tantalum and Niobium. Metallurgist 47, 33–41.

Rodriguez, M.H., Rosales, G.D., Pinna, E.G., Suarez, D.S., 2015. Extraction of niobium and tantalum from ferrocolumbite by hydrofluoric acid pressure leaching. Hydrometallurgy 156, 17–20. https://doi.org/10.1016/j.hydromet.2015.05.006.

Rodriguez, M.H., Rosales, G.D., Pinna, E.G., Suarez, D.S., 2016. Effect of Na + ion on the dissolution of ferrocolumbite in autoclave. Hydrometallurgy 159, 60–64. https://doi.org/10.1016/j.hydromet.2015.10.033.

Ryan, G., Pandit, A., Apatsidis, D., 2006. Fabrication methods of porous metals for use in orthopaedic applications. Biomaterials 27, 2651–2670. https://doi.org/10.1016/j.biomaterials.2005.12.002.

Sanchez-Segado, S., Lahiri, A., Jha, A., 2014. Alkali roasting of bomar ilmenite: rare earths recovery and physico-chemical changes. Open Chem. 13 https://doi.org/10.1515/chem-2015-0033.

Sanchez-Segado, S., Makanyire, T., Escudero-Castejon, L., Hara, Y., Jha, A., 2015. Reclamation of reactive metal oxides from complex minerals using alkali roasting and leaching – an improved approach to process engineering. Green Chem. 17, 2059–2080. https://doi.org/10.1039/C4GC02360A.

Sanchez-Segado, S., Monti, T., Katrib, J., Kingman, S., Dodds, C., Jha, A., 2017. Towards sustainable processing of columbite group minerals: elucidating the relation between dielectric properties and physico-chemical transformations in the mineral phase. Sci. Rep. 7, 18016. https://doi.org/10.1038/s41598-017-18272-3.

Santos, C.A. dos; Zawislak, L.I.; Kinast, E.J.; Antonietti, V.; Cunha, J.B.M. da, 2001. Crystal chemistry and structure of the orthorhombic (Fe,Mn)(Ta,Nb)2O6 family of compounds. Brazilian J. Phys. 31, 616–631.

Tanaka, I., Inoue, R., Kojima, H., Oyamada, R., 1988. Single crystal growth of tantalite ((Fe, Mn)(Ta, Nb)2O6) solid solutions. J. Cryst. Growth 91, 141–146. https://doi.org/10.1016/0022-0248(88)90379-X.

Upadhya K, Yang J, M, H.W., 1997. Advanced Materials for Ultrahigh Temperature Structural Applications above 2000°C.

Vyverberg, K.L., Jaeger, J.M., Dutton, A., 2018. Quantifying Detection Limits and Uncertainty in X-ray Diffraction Mineralogical Assessments of Biogenic Carbonates. J. Sediment. Res. 88, 1261–1275. https://doi.org/10.2110/jsr.2018.63.

Wang, X., Zheng, S., Xu, H., Zhang, Y., 2009. Leaching of niobium and tantalum from a low-grade ore using a KOH roast–water leach system. Hydrometallurgy 98, 219–223. https://doi.org/10.1016/j.hydromet.2009.05.002.

M. A. Wise, P.C., 1996. The crystal chemistry of the tapiolite series. Can. Mineral. 34, 631–647.

Zafrir, M., Aladjem, A., Zilber, R., Ben-Dor, L., 1976. Preparation of a continuous series of solid solutions in the Ta2O5Nb2O5 system. J. Solid State Chem. 18, 377–380. 10.1016/0022-4596(76)90121-3.

Zhou, H., Zheng, S., Zhang, Y., 2005. Leaching of a low-grade niobium–tantalum ore by highly concentrated caustic potash solution. Hydrometallurgy 80, 83–89. https://doi.org/10.1016/j.hydromet.2005.07.006.

Zhu, Z., Cheng, C.Y., 2011. Solvent extraction technology for the separation and purification of niobium and tantalum: A review. Hydrometallurgy 107, 1–12. https://doi.org/10.1016/j.hydromet.2010.12.015.